A newly conceived cylinder measuring machine and methods that eliminate the spindle errors

Alain Vissiere, Hichem Nouira, Mohamed Damak, Olivier Gibaru, Jean Marie David

▶ **To cite this version:**

Alain Vissiere, Hichem Nouira, Mohamed Damak, Olivier Gibaru, Jean Marie David. A newly conceived cylinder measuring machine and methods that eliminate the spindle errors. Measurement Science and Technology, 2012, 23 (9), pp.10. 10.1088/0957-0233/23/9/094015 . hal-01084382

HAL Id: hal-01084382
https://hal.science/hal-01084382

Submitted on 16 Feb 2015

HAL is a multi-disciplinary open access archive for the deposit and dissemination of scientific research documents, whether they are published or not. The documents may come from teaching and research institutions in France or abroad, or from public or private research centers.

L'archive ouverte pluridisciplinaire **HAL**, est destinée au dépôt et à la diffusion de documents scientifiques de niveau recherche, publiés ou non, émanant des établissements d'enseignement et de recherche français ou étrangers, des laboratoires publics ou privés.

A newly conceived cylinder measuring machine and methods that eliminate the spindle errors

A Vissiere[1,2], H Nouira[3,4], M Damak[1,2], O Gibaru[1] and J-M David[1]

[1] Ecole Nationale Supérieure d'Arts & Métiers de Lille (Arts et Métiers ParisTech), (LSIS), 8 Boulevard Louis XIV, 59046 Lille, France
[2] GEOMNIA: Advanced 3D Engineering and Software Solutions, 165 Avenue de Bretagne, EuraTechnologies 59000 Lille, France
[3] Laboratoire National de Métrologie et d'Essais (LNE), Dimensional Metrology Department, 1 Rue Gaston Boissier, 75015 Paris, France

E-mail: hichem.nouira@lne.fr

Abstract
Advanced manufacturing processes require improving dimensional metrology applications to reach a nanometric accuracy level. Such measurements may be carried out using conventional highly accurate roundness measuring machines. On these machines, the metrology loop goes through the probing and the mechanical guiding elements. Hence, external forces, strain and thermal expansion are transmitted to the metrological structure through the supporting structure, thereby reducing measurement quality. The obtained measurement also combines both the motion error of the guiding system and the form error of the artifact. Detailed uncertainty budgeting might be improved, using error separation methods (multi-step, reversal and multi-probe error separation methods, etc), enabling identification of the systematic (synchronous or repeatable) guiding system motion errors as well as form error of the artifact. Nevertheless, the performance of this kind of machine is limited by the repeatability level of the mechanical guiding elements, which usually exceeds 25 nm (in the case of an air bearing spindle and a linear bearing). In order to guarantee a 5 nm measurement uncertainty level, LNE is currently developing an original machine dedicated to form measurement on cylindrical and spherical artifacts with an ultra-high level of accuracy. The architecture of this machine is based on the 'dissociated metrological technique' principle and contains reference probes and cylinder. The form errors of both cylindrical artifact and reference cylinder are obtained after a mathematical combination between the information given by the probe sensing the artifact and the information given by the probe sensing the reference cylinder by applying the modified multi-step separation method.

Keywords: dimensional metrology, precision engineering, multi-step and reversal error separation methods

(Some figures may appear in colour only in the online journal)

1. Introduction

This work is in direct relation to the LNE project whose objective is to develop a new ultra-high precision geometric measuring machine, with better metrological performance than existing machines, to measure form error of cylindrical artifacts such as standard rings, plug gauges, spheres and piston–cylinder assemblies. The uncertainty level targets are 5 nm for the roundness assessment, 10 nm for the straightness assessment and 20 nm for the cylindricity assessment. This has

[4] Author to whom any correspondence should be addressed.

led LNE to design an ultra-high accuracy machine described in [1] on which the present work is based. This targeted level of uncertainty is a real challenge in dimensional metrology in comparison with the current best uncertainties reported in the BIPM's Key Comparison Database (KCDB) [2]. The NMIs' (National Metrology Institutes) uncertainty values published in the KCDB are obtained using modified conventional machines [3–6]. The performance of these machines is limited mainly by the quality and stability of the guiding systems as well as the mechanical stability of the supporting structure. To improve the measurement, it is essential to identify the motion error of the mechanical guiding elements by applying some standard methods such as the reversal, multi-step and multi-probe error separation methods. These methods allow separation of form error and motion error.

To achieve the targeted levels of uncertainty, the new device has a dissociated metrology technique (DMT)-based architecture as defined in [7, 8] and applied in many machines developed by LNE [9–11]. The performance of the equipment is only limited by the performance of the probe sensors and the stability of the reference elements.

In this paper, we will briefly analyze the sources of inherent error in conventional and industrial machines for cylindricity measurement, as well as the limits of error compensation on these machines. The mathematical development of both standard and modified multi-step methods will be introduced. A numerical comparison between these two methods will be presented and discussed. The modified reversal method will also be detailed here. Based on this approach, we will be able to justify the evolution from a conventional architecture to an architecture integrating the DMT technique.

2. Conventional equipment for cylindricity measurement

2.1. Analysis of conventional equipment

On conventional machines, measurement is carried out through the comparison of the form of the artifact with high quality motion. The roundness of an artifact is measured by subjecting it to a high quality rotation and by monitoring its surface with a fixed probe. Based on the definition of the 'metrology loop', which is a reference frame for displacement measurement, independent of the instrument base [12, 13], conventional machines typically have a serial metrology loop, representing a conceptual line going through all solids, joints and probes. Serial structures are made of a succession of solids joined by linkages defining the degree of freedom of each solid. Any uncontrolled dimensional modification has an impact on the final uncertainty.

Dimensional changes of the metrology loop are divided into two categories. The first one consists of the correctable and repeatable errors such as errors in metrological scale and encoding systems, movement errors caused by the guide surfaces' form and roughness errors, errors of relative position between movements and errors caused by elastic deformation of components and guides under the effect of stresses.

Figure 1. Conventional measurement machine: KOSAKA.

These errors may be identified by previous characterization experiments: testing stabilities, measuring arm deformations by using a strain gauge and applying standard error separation methods. The second category consists of the uncorrectable modifications of the metrology loop, which are mainly caused by non-repeatable (random) errors of guiding systems (commonly referred to as asynchronous (random) motion errors [13]), differential thermal expansions, vibrations and wear. These errors cannot be compensated by using the above-mentioned methods.

An example of a conventional and industrial geometry measurement machine is presented in figure 1. Figure 2 describes the kinematic scheme of this machine and illustrates the metrology loop which reflects the metrological performance of the machine. Analysis of the metrology loop clearly shows that the quality of the assessment strongly depends on the quality and stability of motion (air bearing spindle and aerostatic linear guiding system), the stability of the instrument base and the performance of the probe.

2.2. Standard error separation methods

These methods are usually used to qualify, analyze and calibrate a measurement instrument. The recorded dataset combines errors due to the synchronous and asynchronous motion errors (systematic and random motion errors) of the spindle and the linear guiding system and errors due to the out-of-roundness/straightness of an artifact, which cannot be ignored. Three methods can be introduced:

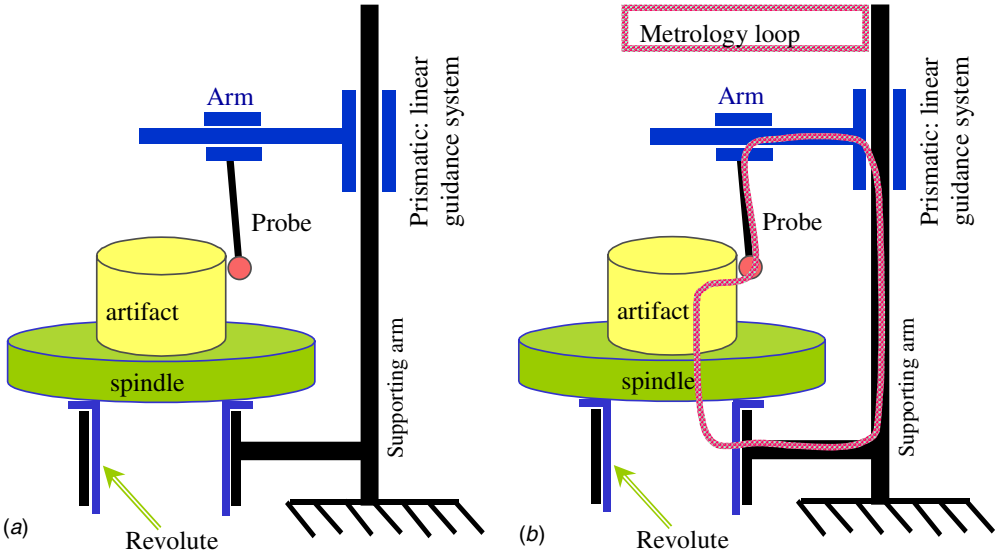

Figure 2. (*a*) Kinematics diagram of a conventional machine, (*b*) identification of the metrology loop (represented by the pink line) which passes through mechanical guiding and supporting elements.

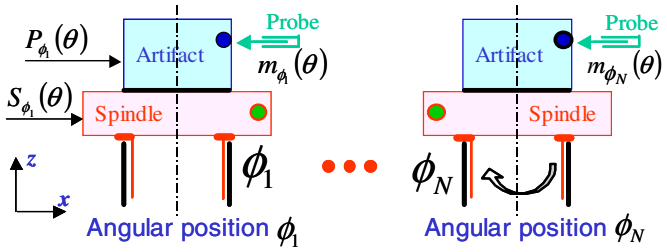

Figure 3. Description of the classical multi-step separation method. Application of the multi-step method implies carrying out N measurements of the spindle with N angularly spaced steps. The application of this method allows us to separate the part form error from the spindle motion error.

- *Reversals*: this method requires only two measurements. Both the artifact and the probe must be moved between measurements [13–16].
- *Multi-probe method*: this method uses at least three probes to simultaneously measure error components. In this case, neither the probes nor the artifact are moved, but all must be properly arranged to measure the same track on the artifact [13, 16–20].
- *Multi-step method*: this method requires many measurements for each spindle error component. Here we do not move the probe, but instead we rotate the artifact by equally-spaced angular increments [13, 16, 21, 22].

2.3. Standard multi-step error separation method: roundness

The multi-step method is a classical error separation technique in which the artifact is indexed in angularly spaced increments without moving the probe. Figures 3 and 4 show a diagram of the multi-step method in which measurements are made for each angular position and the artifact is indexed N angular increments of ϕ_k ($k = 1, \ldots, N$, and $\phi_1 = 0$) relative to the spindle. A single fixed probe measures the form variation at the same orientation angle for all angular increments of the artifact. Thus, each measurement $m_{\phi_i}(\theta)$ contains only the shifted spindle synchronous radial error motion $S_\phi(\theta)$ and the part form error $P_\phi(\theta)$. With this method we assume that the response of the probe is perfect and does not contain noise or linearity error or any other kind of defect. We also assume that the spindle and the linear guiding systems do not contain any asynchronous motion errors.

Based on figure 3 and on the previous assumptions, each of the recorded measurements can be written in the form of equations (1)–(3), which reflect the combined contribution

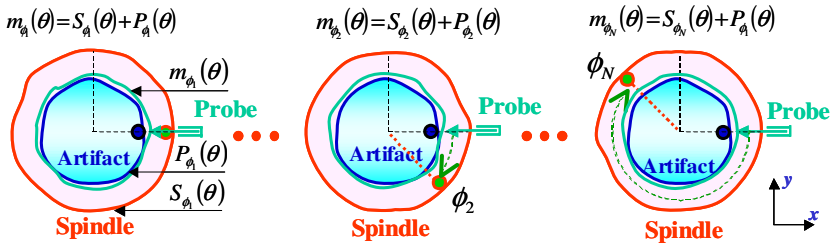

Figure 4. Schematic description of the multi-step separation method and error signals. Application of the multi-step method implies carrying out N measurements of the spindle with N angularly spaced steps. Here the colors blue, red and green correspond respectively to the schematic roundness of the artifact, the spindle and the probe.

of the synchronous radial motion error of the spindle and the artifact form error. For N recorded measurement results, summing and solving equations for the radial motion error of the spindle gives equation (4). The form error of the artifact can be expressed as a Fourier series (equation (5)).

$$m_{\phi_1}(\theta) = S_{\phi_1}(\theta) + P_{\phi_1}(\theta), \tag{1}$$

$$m_{\phi_2}(\theta) = S_{\phi_2}(\theta) + P_{\phi_1}(\theta), \tag{2}$$

$$\begin{aligned} m_{\phi_N}(\theta) &= S_{\phi_N}(\theta) + P_{\phi_1}(\theta) \\ &= S_{\phi_1}(\theta + N\phi) + P_{\phi_1}(\theta), \end{aligned} \tag{3}$$

$$\begin{aligned} \sum_{k=1}^{N} m_{\phi_k}(\theta) &= \sum_{k=1}^{N} P_{\phi_1}(\theta) + \sum_{k=1}^{N} S_{\phi_1}(\theta + k\phi) \\ &= NP_{\phi_1}(\theta) + \sum_{k=0}^{N-1} S_{\phi_1}(\theta + k\phi), \end{aligned} \tag{4}$$

$$S_{\phi_j}(\theta) = \sum_{j=1}^{\infty} A_j^1 \cos(j\theta) + A_j^2 \sin(j\theta). \tag{5}$$

Averaging measurement results separates the motion error of the spindle from the artifact form error, except at frequencies that are harmonics of the number of angular steps (v) (equation (6)). For the ultra-high precision air bearing spindle, the synchronous radial motion errors are sub-micrometric. Thus, the artifact errors occurring at these higher harmonics and spindle errors can be approximated by the simple model in equation (7). Calculation of the spindle synchronous radial motion error requires taking an individual trace and subtracting the artifact error, leading to equation (8).

$$\begin{aligned} P_{\phi_1}(\theta) &= \frac{1}{N} \sum_{k=1}^{N} m_{\phi_k}(\theta) \\ &\quad - \frac{1}{N} \sum_{k=1}^{N} \sum_{j=1}^{\infty} (B_j \, \mathrm{e}^{ij(\theta + k\phi)} + C_j \, \mathrm{e}^{-ij(\theta + k\phi)}), \end{aligned} \tag{6}$$

$$P(\theta) = P_{\phi_1}(\theta) \approx \frac{1}{N} \sum_{j=1}^{N} m_{\phi_j}(\theta), \tag{7}$$

$$S_{\phi_k}(\theta + k\phi) = m_{\phi_k}(\theta) - P(\theta). \tag{8}$$

2.4. Roundness simulation: multi-step method

Numerical simulation of the previously described method corresponds to the separation between the simulated rotational motion error and the simulated form error (roundness). The simulated spindle signal contains synchronous and asynchronous errors. The amplitudes of the synchronous error motion vary between 2 and 25 nm with less than 31 undulations per revolution (upr). The asynchronous spindle motion error is generated by MATLAB and corresponds to a white noise signal with maximum amplitude of 25 nm. The simulated part form error contains harmonic errors with amplitude variations between 0.1 and 0.9 μm and less than 37 upr.

Thirty-three indexed angular equally-spaced steps are considered. All errors are introduced to the example and the algorithm is applied to separate part form error and spindle radial motion error. For this simulation, angular positioning errors are ignored because there are methods allowing identification of this kind of error which are well presented in [21, 22]. Simulated and recalculated results are presented in figures 4(*a*)–(*d*) and show that residuals between both simulated and recalculated part form and motion errors are always high.

Mathematically, the synchronous motion error is made up of harmonics that occur at integer multiples of the rotational frequency of the spindle. Conversely, the asynchronous motion error is the portion that does not occur at integer multiples of the rotational frequency. Based on this remark, applying the discrete Fourier transformation (DFT) to the recalculated motion error signal (figure 5(*c*)) allows us to separate the synchronous motion error from a portion of the asynchronous motion error. The remaining asynchronous motion error is combined with the portion of the signal involving form error. As a consequence, it is always necessary to apply the DFT to the recalculated part form error in order to remove the remaining asynchronous motion error [13, 16]. To avoid applying the DFT twice, it is possible to apply the DFT to the combined signal $m_{\phi_i}(\theta)$ and therefore obtain a signal which only contains the part form error and the synchronous motion error. It is also important to remove the fundamental component that is related to the misalignment of the artifact. All these remarks mean that the employed technique is not really functional for measurements with accuracy at the nanometer level.

3. Architecture of the new geometric measuring machine

3.1. Basic concept of the machine

The concept of the machine is based on the DMT principle which consists in dissociating the metrology structure from the supporting structure. This allows components of the metrology structure to be employed only for measuring and probing purposes. Application of this principle makes it possible to avoid deformations of the metrology loop caused by unpredictable loads. The metrological structure only has to bear its own weight. Linkages between components of the metrology loop are ensured by probes, which are much better than mechanical joints. The redundancy of the information obtained through an increase in the number of probes improves the quality and reliability of measurements, and is even a permanent means of auto-verification. Another advantage when applying the dissociated metrological principle is the reduction of the effect of environmental disturbances, especially thermal disturbances, since it is usually possible to design a symmetrical machine equipped with many probing elements.

The philosophy of the machine under development is close to that of the PTB (NMI of Germany) machine [4], which is especially used for measuring diameters. The architecture of the machine is based on the comparison of two surfaces: a reference cylinder and a cylindrical artifact, which gets rid of the quality of motion of the mechanical guiding elements

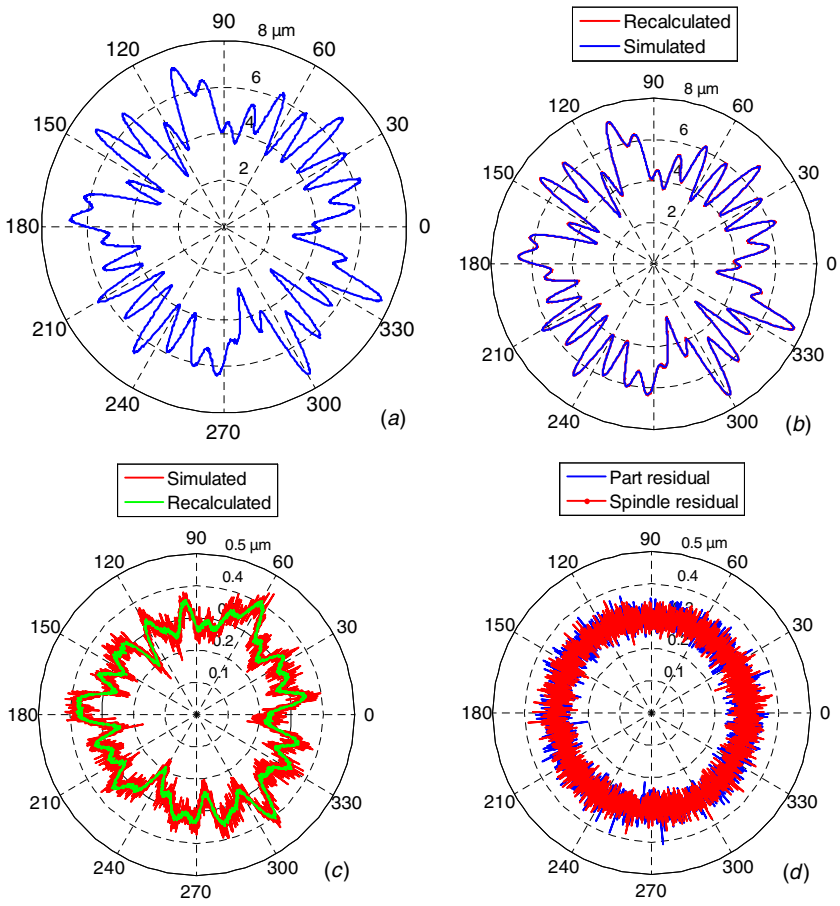

Figure 5. Simulation of the classical multi-step separation method (synchronous and asynchronous spindle error motion is considered). (*a*) An example of combination of both the simulated part form error and simulated synchronous and asynchronous spindle motion errors. (*b*) Simulated and recalculated part form error by applying the classical multi-step separation method. (*c*) Simulated and recalculated synchronous and asynchronous spindle motion error by applying the classical multi-step separation method. (*d*) Illustration of residuals between simulated and recalculated signals by applying the classical multi-step separation method.

(spindle and linear guiding systems). The test cylinder is located inside the hollow reference cylinder. Eight or more contact-less probes (capacitance sensors [13, 23–25]) sense the reference cylinder, and up to four probes sense the artifact. The concept of the machine is completely symmetric and perfectly respects the Abbe principle. The metrology loop goes only through reference and probing elements. As a consequence, measurements are never influenced by the quality of motion of mechanical guiding elements and are only affected by the performance of sensing elements as well as by the stability of reference elements (figure 6). Calibration of all probes of the machine is automatic and carried out *in situ* over a 90 μm travel range by using the nanometric piezoelectric actuators. Calibration of the proposed machine is based on the use of a modified multi-step form error separation technique allowing separation between the form errors of both the reference cylinder and cylindrical artifact. This operation is time consuming, that is why it is performed using an entirely automated indexer. More details concerning the operation, architecture and design of the new geometric measuring machine can be found in [26–28].

3.2. Modified multi-step error separation method: roundness

Calibration of the ultra-high precision machine corresponds to the calibration of the entire two dimensional (2D) reference cylinder, as shown in figure 6. To this purpose, the modified multi-step error separation method is applied at many different heights by performing N angular spaced shifts between the two surfaces (reference cylinder and artifact). Each dataset delivered by the probe combines both the form error and the motion error. The final measurement, which corresponds to the difference between the two datasets and is given by both the measuring and reference probes, gives the deviation between the two functions of roundness form of the two surfaces.

Consider the example presented in figure 7 in which only two probes are taken into account: for roundness measurement, the probe sensing the reference cylinder gives an indication $m^R_{\phi_k}(\theta)$ which is a mix between the reference cylinder form error $P^R_{\phi_k}(\theta)$ and the spindle motion error (equation (9)). The probe sensing the part gives a second indication $m^T_{\phi_k}(\theta)$ which is a mix between the part form error $P^T_{\phi_1}(\theta)$ and the same spindle motion error (equation (9)). The spindle motion error contains both synchronous errors $S^S_{\phi_k}(\theta)$ and asynchronous errors $S^{\mathrm{As}}_{\phi_k}(\theta)$:

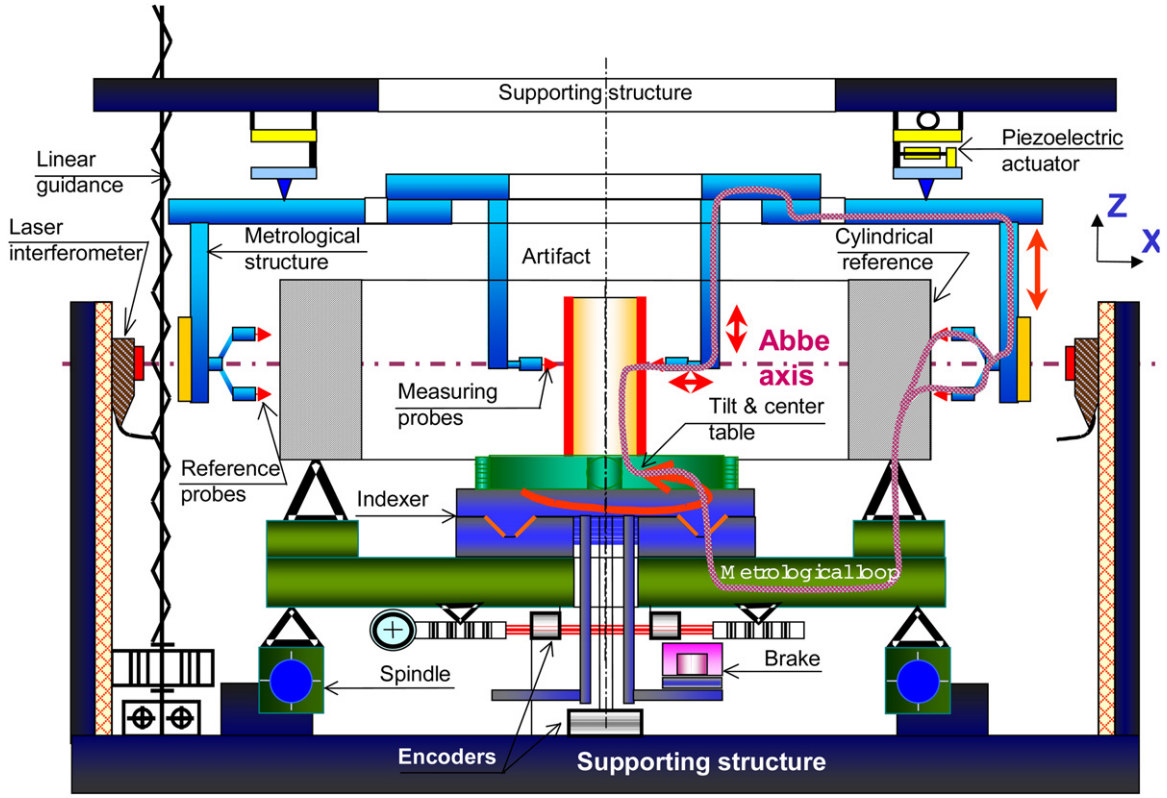

Figure 6. Architecture of the geometric measuring machine. The presented architecture perfectly respects both the dissociated metrology structure and Abbe principles. The pink line (▬▬▬) represents the metrology loop which passes through reference and probing elements. Only one side of the metrology loop is presented in the figure, the second metrology loop is perfectly symmetric. The metrology loop is never affected by the quality of motion errors of mechanical guiding elements. More details concerning the architecture of this machine are given in [1, 27, 28].

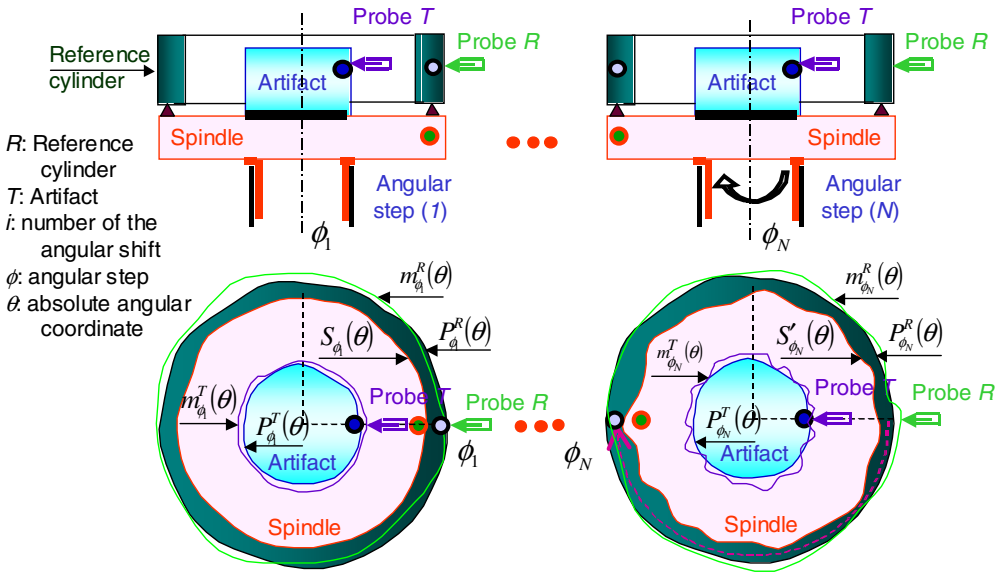

Figure 7. Schematic description of the modified multi-step separation method: case device with only two probes. To apply this method, N measurements should be carried out in which the spindle is indexed in angularly spaced increments without moving the probe or the artifact. The colors red, blue, green and violet correspond respectively to the spindle motion error, the part form error, the signal given by the probe R and the signal given by the probe T.

$$
\begin{aligned}
m^R_{\phi_k}(\theta) &= S^S_{\phi_k}(\theta) + S^{\mathrm{As}}_{\phi_k}(\theta) + P^R_{\phi_k}(\theta),\\
m^T_{\phi_k}(\theta) &= S^S_{\phi_k}(\theta) + S^{\mathrm{As}}_{\phi_k}(\theta) + P^T_{\phi_1}(\theta),\\
\text{with}\quad & k = 1, \ldots, N.
\end{aligned}
\tag{9}
$$

For each angular increment, the difference between the information given by the reference and the information given by the measuring probes gives a signal $D^{(T-R)}_{\phi_k}(\theta)$ which does

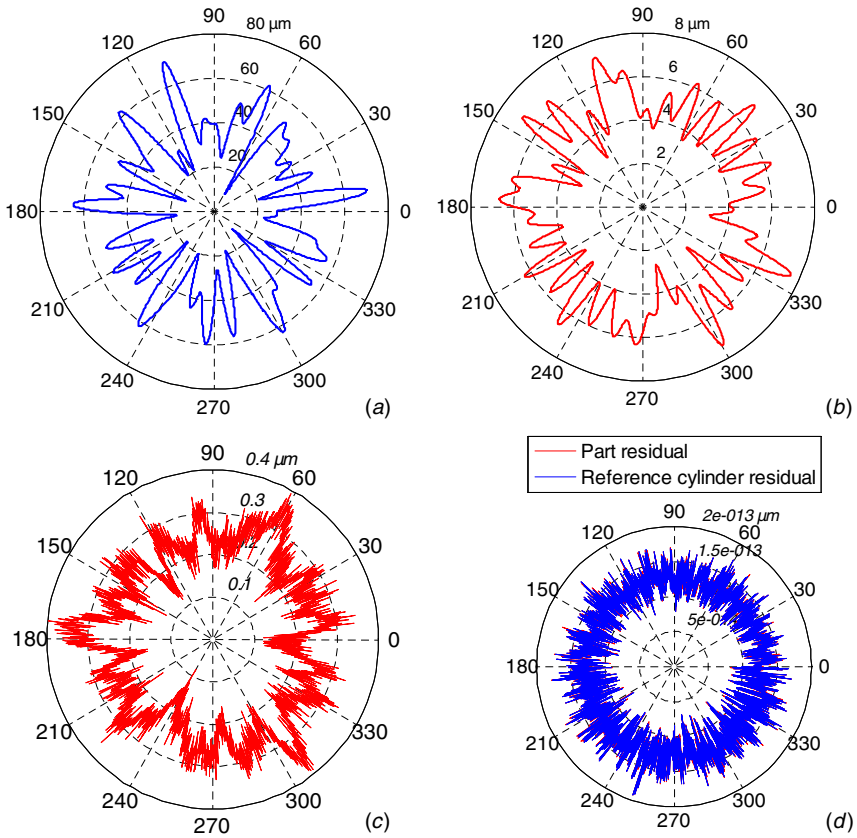

Figure 8. Simulation of the modified multi-step separation method (synchronous and asynchronous spindle error motion is considered, linearity error probe is ignored). (*a*) Illustration of both simulated and recalculated reference cylinder form errors by application of the modified multi-step separation method. The two signals are very similar which explains the negligible value of the residual (figure 8(*d*)). (*b*) Illustration of both simulated and recalculated part form errors by application of the modified multi-step separation method. The two signals are very similar which explains the negligible value of the residual (figure 8(*d*)). (*c*) Simulated synchronous and asynchronous spindle error motion. (*d*) Residuals between the simulated and recalculated signals by application of the modified multi-step separation method.

not take into account the synchronous and the asynchronous spindle motion errors (equations (10) and (11)):

$$D_{\phi_k}^{(T-R)}(\theta) = m_{\phi_k}^{T}(\theta) - m_{\phi_k}^{R}(\theta) = P_{\phi_1}^{T}(\theta) - P_{\phi_k}^{R}(\theta), \quad (10)$$

$$\sum_{k=1}^{N} D_{\phi_k}^{(T-R)}(\theta) = NP_{\phi_1}^{T}(\theta) - P_{\phi_k}^{R}(\theta + k\phi). \quad (11)$$

By solving the problem, we obtain the part form error $P^T(\theta)$ and the reference cylinder form error $P^R(\theta)$, which are expressed in equations (12) and (13):

$$P^{T}(\theta) = P_{\phi_1}^{T}(\theta) \approx \frac{1}{N}\sum_{k=1}^{N} D_{\phi_k}^{(T-R)}(\theta), \quad (12)$$

$$P_{\phi_k}^{R}(\theta + k\phi) = P^{T}(\theta) - D_{\phi_k}^{(T-R)}(\theta). \quad (13)$$

The limitation of this method is that an error with a periodicity of N periods per turn cannot be detected. This problem could be avoided by making the measurement twice: once with N angular spacing shifts, and a second time with P angular spacing shifts, N and P being two coprime integers (for example $N = 41$ and $P = 47$). The modified multi-step method is sensible to the resolution and the performance of both the reference probes and the measuring probes, which have to be similar in order to remove all errors caused by the motion defaults.

3.3. Roundness simulation: modified multi-step method

The modified multi-step error separation method is applied in order to dissociate the simulated part and reference form errors. To achieve this, we need to simulate two form errors $\left(m_{\phi_k}^{T}(\theta)\right.$ and $\left.m_{\phi_k}^{R}(\theta)\right)$ and both synchronous $S_{\phi_k}^{S}(\theta)$ and asynchronous $S_{\phi_k}^{\mathrm{As}}(\theta)$ spindle motion errors as described previously. All simulations are performed with 33 indexed angularly spaced steps. The simulated spindle motion error contains exactly the same harmonic errors as in the example presented in section 2.4: the amplitudes vary between 2 and 25 nm and there are less than 25 upr. The simulated asynchronous spindle motion errors correspond to a white noise with maximum amplitude of 25 nm. The simulated part form error signal also contains harmonic errors similar to the example presented in section 2.4, with amplitude variations between 0.1 and 0.9 μm and the same number of undulations per revolution: less than 37 upr. Finally, the simulated reference cylinder form error signal contains harmonic errors with amplitude variations between 0.1 and 10 μm and less than 31 upr. For this simulation, the linearity error of the probes is ignored. To complete the simulation, each form error signal (part and reference cylinder (figures 8(*a*) and (*b*)) is combined with both

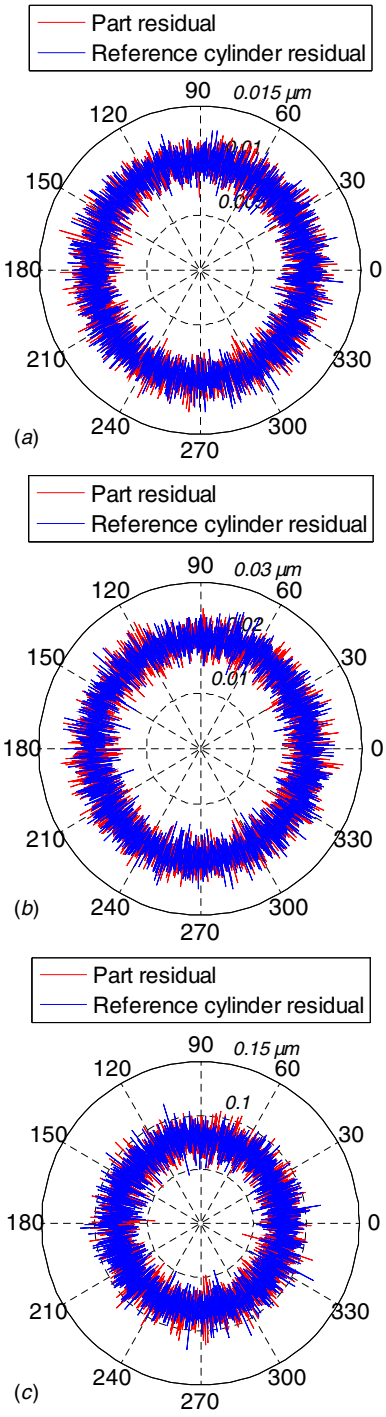

Figure 9. Investigation of the impact of the nonlinear residual error of the probe. These figures illustrate that the increase in nonlinear residual errors cause the residual between the simulated and recalculated signals to increase as well, and inversely. (*a*) Illustration of residuals between the simulated and recalculated signals by application of the modified multi-step method. The nonlinear residual error of the probe is equal to 1 nm. (*b*) Illustration of residuals between the simulated and recalculated signals by application of the modified multi-step method. The nonlinear residual error of the probe is equal to 2 nm. (*c*) Illustration of residuals between the simulated and recalculated signals by application of the modified multi-step method.The nonlinear residual error of the probe is equal to 10 nm.

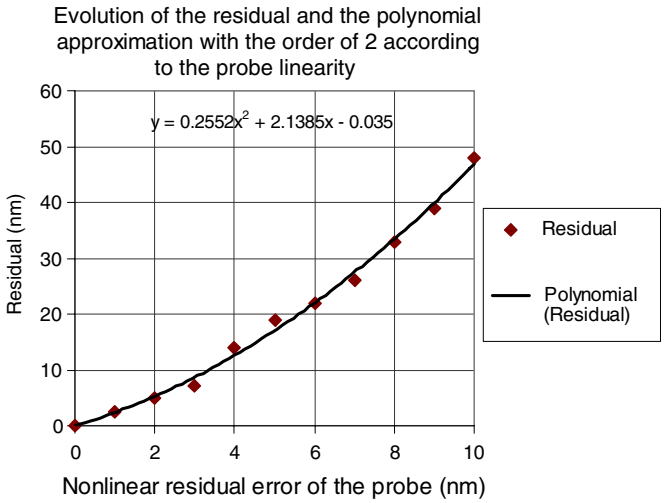

Figure 10. Summary of the evolution of the residual and of the polynomial approximation according to the nonlinear residual error of the probe, which is quadratic.

synchronous and asynchronous spindle motion error signals to obtain $m^T_{\phi_k}(\theta)$ and $m^R_{\phi_k}(\theta)$ signals (figure 8(*c*)).

The described method in equations (10)–(13) is applied and the obtained residuals between the simulated and recalculated part and the reference cylinder form errors are presented in figure 8(*d*). We observe that both residuals are within the order of 10^{-13}, which corresponds to the resolution of Matlab software. These results confirm that the modified multi-step method gets rid of the synchronous and asynchronous motion errors. Based on this last remark, application of the dissociated metrological structure principle makes it possible to equip the new ultra-high precision device with low-cost mechanical guiding elements.

As mentioned before, the modified multi-step method is mainly influenced by the performance of the probes, especially the nonlinear residual error. This error corresponds to deviation of the dataset from the linear or quadratic model. This is achieved by subtracting the linear or quadratic approximation from the actual data, leaving only the nonlinear component of data points [23, 24].

In order to understand the impact of this parameter on results, a second simulation is run with many levels of nonlinear residual error of the probes $E_{\phi_k}(\theta)$, ranging between 1 and 10 nm. Similarly, the same maximal nonlinear residual error amplitude is considered for both the reference and the measuring probes, but their distribution (as a white noise) is different (equation (14)):

$$\begin{aligned} m^R_{\phi_k}(\theta) &= S^S_{\phi_k}(\theta) + S^{\mathrm{As}}_{\phi_k}(\theta) + P^R_{\phi_k}(\theta) + E^R_{\phi_k}(\theta), \\ m^T_{\phi_k}(\theta) &= S^S_{\phi_k}(\theta) + S^{\mathrm{As}}_{\phi_k}(\theta) + P^T_{\phi_1}(\theta) + E^T_{\phi_k}(\theta). \end{aligned} \tag{14}$$

The obtained results are presented in figures 9(*a*)–(*c*) and reveal that residuals, which are similar for both the part and the reference cylinder, increase from zero when nonlinear residual errors are considered negligible, to 50 nm when the amplitude of the nonlinear residual error is close to 10 nm. Approximation of the observed residual amplitudes according to nonlinear residual errors shown in figure 10 presents a parabolic tendency. However, residual

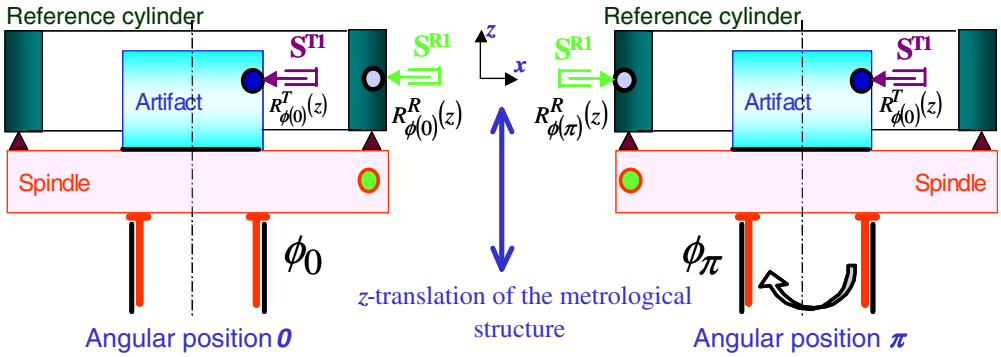

Figure 11. Schematic description of the modified reversal separation method. S^{T1} and S^{R1} represent the designations of respectively measuring part probe and reference probe. To perform this technique, two straightness measurements should be carried out. The first straightness measurement must be carried out for angular position 0 and the two probes must be in the same corner and direction. The second measurement must be carried out for angular position π. For this configuration, both the reference probe and reference cylinder are shifted by the angle of π. The direction of the two probes becomes opposite. To perform this method, the metrological structure should ensure two degrees of freedom (z-translation and z-rotation). The z-rotation of the metrological structure can cause additional positioning errors and this solution should be avoided.

values can be reduced and the targeted accuracy can be attained if the spatial redundancy principle is applied, as shown in figure 6. Both form errors are made up of harmonics occurring at integer multiples of the rotational frequency of the spindle. The nonlinear residual error is the fraction not occurring at integer multiples of the rotational frequency. Based on these remarks, the application of the DFT to the mixed signal $D^{(T-R)}_{\phi_k}(\theta)$ allows separation of the form error from the nonlinear residual error.

3.4. Modified reversal method: identification of straightness

The standard reversal method is well detailed in [14, 15] and allows separation of straightness and motion error. Hence, this section is focused only on the modified reversal method allowing separation of the artifact and reference cylinder form errors.

Considering the case presented in figure 11, $m^T_\phi(z)$, $m^R_\phi(z)$, $R^T_\phi(z)$, $R^R_\phi(z)$, $L^S_\phi(z)$ and $L^{\mathrm{As}}_\phi(z)$ represent respectively the measurement given by the measuring probe, the measurement given by the reference probe, the generator straightness of the artifact, the generator straightness of the reference cylinder, the synchronous motion error of the vertical linear guiding system and the asynchronous motion error of the same vertical linear guiding system. z represents the z-axis and ϕ represents the angular position.

Each measurement mingles form error of straightness and both synchronous and asynchronous motion errors of the vertical linear guiding system. To obtain the generator straightness, we need two different measurements at angular positions 0 and π, as shown in figure 11. For position 0, formulations are presented in equation (15):

$$\begin{aligned} m^T_{\phi(0)}(z) &= R^T_\phi(z) + L^S_{\phi(0)}(z) + L^{\mathrm{As}}_{\phi(0)}(z), \\ m^R_{\phi(0)}(z) &= R^R_\phi(z) + L^S_{\phi(0)}(z) + L^{\mathrm{As}}_{\phi(0)}(z). \end{aligned} \tag{15}$$

The next step is shifting both the reference probe and reference cylinder, which are associated with the spindle, by an angular increment of π. The angular position of the test standard remains unchanged. Formulations linked to this second position are presented in equation (16):

$$\begin{aligned} m^T_{\phi(\pi)}(z) &= R^T_\phi(z) + L^S_{\phi(\pi)}(z) + L^{\mathrm{As}''}_{\phi(\pi)}(z), \\ m^R_{\phi(\pi)}(z) &= R^R_\phi(z) - L^S_{\phi(\pi)}(z) - L^{\mathrm{As}''}_{\phi(\pi)}(z). \end{aligned} \tag{16}$$

The difference and the sum of the information given by the reference and measuring probes for the first and second angular positions provide respectively two signals ($\Delta^{(T-R)}_{\phi(0)}$ and $\Delta^{(T+R)}_{\phi(0)}$), which are independent of the motion error and can only be influenced by the nonlinear residual error of the probes (equation (17)):

$$\begin{aligned} \Delta^{T-R}_{\phi(0)}(z) &= m^T_{\phi(0)}(z) - m^R_{\phi(0)}(z) = R^T_\phi(z) - R^R_\phi(z), \\ \Delta^{T+R}_{\phi(\pi)}(z) &= m^T_{\phi(\pi)}(z) + m^R_{\phi(\pi)}(z) = R^T_\phi(z) + R^R_\phi(z). \end{aligned} \tag{17}$$

The linear combination of the last two signals allows finding the generator straightness of the part and the reference cylinder (equation (18)):

$$\begin{aligned} R^T_\phi(z) &= \frac{\Delta^{(T-R)}_{\phi(0)}(z) + \Delta^{(T+R)}_{\phi(\pi)}(z)}{2}, \\ R^R_\phi(z) &= \frac{\Delta^{(T+R)}_{\phi(\pi)}(z) - \Delta^{(T-R)}_{\phi(0)}(z)}{2}. \end{aligned} \tag{18}$$

In order to apply the modified reversal method, the metrological structure should ensure two degrees of freedom: one translation along the z-axis and one rotation around the same z-axis. Unfortunately, this is very complex to create and can introduce additional positioning error. As a solution, it is easier and cheaper to add opposite probes as shown in figure 12. For angular positions 0 and π, each probe gives information respectively as described in equations (19) and (20). With the second configuration, the metrological structure should ensure only one degree of freedom (translation along the z-axis).

$$\begin{aligned} m^{T1}_{\phi(0)}(z) &= R^{T1}_\phi(z) + L^S_{\phi(0)}(z) + L^{\mathrm{As}}_{\phi(0)}(z), \\ m^{R1}_{\phi(0)}(z) &= R^{R1}_\phi(z) + L^S_{\phi(0)}(z) + L^{\mathrm{As}}_{\phi(0)}(z), \\ m^{T2}_{\phi(0)}(z) &= R^{T2}_\phi(z) - L^S_{\phi(0)}(z) - L^{\mathrm{As}}_{\phi(0)}(z), \\ m^{R2}_{\phi(0)}(z) &= R^{R2}_\phi(z) - L^S_{\phi(0)}(z) - L^{\mathrm{As}}_{\phi(0)}(z); \end{aligned} \tag{19}$$

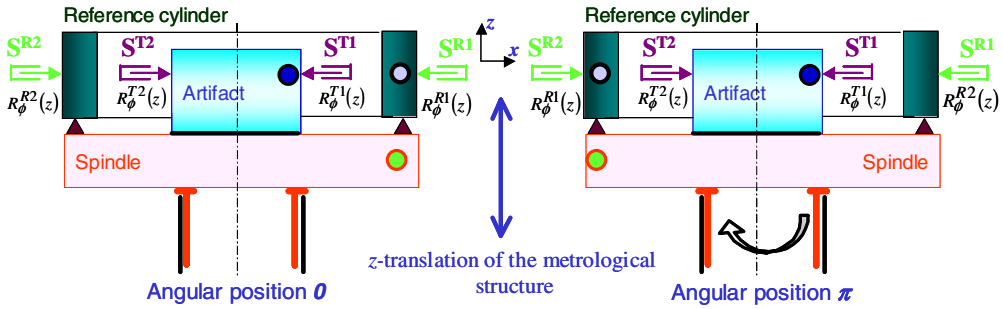

Figure 12. Schematic description of the modified and performed reversal separation method. S^{T1} and S^{T2} represent the designations of measuring part probes and S^{R1} and S^{R2} represent the designations of reference probes. To perform this second configuration, two straightness measurements should be carried out. The first straightness measurement must be carried out for angular position 0. The second test must be carried out for angular position π. For this configuration, only the reference cylinder is shifted by the angle of π and the probes remain unchanged. To perform this second method, the metrological structure should ensure only one degree of freedom (z-translation).

$$\begin{aligned}
m^{T1}_{\phi(\pi)}(z) &= R^{T1}_{\phi}(z) + L^{S}_{\phi(\pi)}(z) + L^{As''}_{\phi(\pi)}(z),\\
m^{R1}_{\phi(\pi)}(z) &= R^{R2}_{\phi}(z) + L^{S}_{\phi(\pi)}(z) + L^{As''}_{\phi(\pi)}(z),\\
m^{T2}_{\phi(\pi)}(z) &= R^{T2}_{\phi}(z) - L^{S}_{\phi(\pi)}(z) - L^{As''}_{\phi(\pi)}(z),\\
m^{R2}_{\phi(\pi)}(z) &= R^{R1}_{\phi}(z) - L^{S}_{\phi(\pi)}(z) - L^{As''}_{\phi(\pi)}(z).
\end{aligned} \tag{20}$$

Linear combination of the formulations as shown in equation (21) never depends on the motion errors and allows obtaining four generator straightness results out of two measurements (equation (22)). To obtain several generator straightness, this method should be applied several times with different angular positions between 0 and π.

$$\begin{aligned}
\Psi_1(z) &= m^{T1}_{\phi(0)}(z) - m^{R1}_{\phi(0)}(z) = R^{T1}_{\phi}(z) - R^{R1}_{\phi}(z),\\
\Psi_2(z) &= m^{T1}_{\phi(\pi)}(z) + m^{R2}_{\phi(\pi)}(z) = R^{T1}_{\phi}(z) + R^{R1}_{\phi}(z),\\
\Psi_3(z) &= m^{T2}_{\phi(0)}(z) - m^{R2}_{\phi(0)}(z) = R^{T2}_{\phi}(z) - R^{R2}_{\phi}(z),\\
\Psi_4(z) &= R^{T2}_{\phi(\pi)}(z) + m^{R1}_{\phi(\pi)}(z) = R^{T2}_{\phi}(z) + R^{R2}_{\phi}(z);
\end{aligned} \tag{21}$$

$$\begin{aligned}
R^{T1}_{\phi}(z) &= \frac{\Psi_2(z) + \Psi_1(z)}{2},\\
R^{R1}_{\phi}(z) &= \frac{\Psi_2(z) - \Psi_1(z)}{2},\\
R^{T2}_{\phi}(z) &= \frac{\Psi_4(z) + \Psi_3(z)}{2},\\
R^{R2}_{\phi}(z) &= \frac{\Psi_4(z) - \Psi_3(z)}{2}.
\end{aligned} \tag{22}$$

4. Conclusion

This paper introduces the standard multi-step separation method, which is used to separate the synchronous (systematic) spindle motion error and the artifact form error. To obtain complete measurements with accuracy at the nanometer level, the spindle should present the ultra-high class of motion, which is extremely expensive.

The modified multi-step separation method developed in this paper is in direct relation to our current development of a new ultra-high precision machine based on the concept of dissociated metrological structure. The mathematical formulations presented reveal that the modified multi-step method is never influenced by the quality of motion (synchronous (systematic) and asynchronous (random) motion errors) of mechanical guiding elements, but is only limited by the performance of the probes used and the stability of reference elements (cylinder).

A numerical simulation of both standard and modified multi-step methods is completed and confirms the previous remarks. Comparison of the two methods confirms that the second method is more adapted for measurement with ultra-high level of uncertainty (a few nanometers). However, for roundness measurement the reversal method is not developed here because it is a particular case of the multi-step method.

Finally the mathematical formulations are also developed in order to determine the generator straightness by using the reversal separation error method. The mathematical formulations show clearly that the operation of the new device is never affected by the motion errors.

References

[1] Vissiere A *et al* 2012 Concept and architecture of a new apparatus for cylindrical form measurement with nanometric level of accuracy *Meas. Sci. Technol.* **23** 094014

[2] http://kcdb.bipm.org/AppendixC/search.asp?branch=L/DimMet

[3] Lüdicke F *et al* 2000 Form and length measurement by use of a modified commercial form measurement instrument *Proc. 15th ASPE Annual Meeting*

[4] Neugebauer M *et al* 1997 A new comparator for measurement of diameter and form of cylinders, spheres and cubes under clean-room conditions *Meas. Sci. Technol.* **8** 849–56

[5] Jusko O *et al* 2009 Dimensional calibration techniques for pressure balances to be used in the new determination of the Boltzmann *Informative Bulletin of The Interamerican Metrology System—OAS*

[6] Neugebauer M 2001 Uncertainty analysis for roundness measurements by the example of measurements on a glass hemisphere *Meas. Sci. Technol.* **12** 68–76

[7] David J M 1989 Renault Automation on 'Machine à mesurer par coordonnées' *Patent* (publication no FR 2627582-19890825)

[8] David J M and Coorevits T 1993 Les limites de la correction par logiciel des erreurs de géométrie des M.M.T. Définition d'une architecture nouvelle de machine *6th Int. Conf. of Metrology*

[9] Leleu S 2000 Contribution à l'évaluation des angles, conception, réalisation et validation d'un plateau pivotant

de très haute précision *PhD Thesis* Arts et Métiers ParisTech, France
[10] Lahousse L *et al* 2005 Application d'une nouvelle conception d'architecture à une machine de mesure de résolution nanométrique *Rev. Fr. Métrol.* **4** 35–43
[11] Ducourtieux S and Poyet B 2011 Development of a metrological atomic force microscope with minimized Abbe error and differential interferometer based real-time position control *Meas. Sci. Technol.* **22** 094010
[12] Leach R K 2009 *Fundamental Principles of Engineering Nanometrology* (Oxford: William Andrew)
[13] Marsh E R 2008 *Precision Spindle Metrology* (Lancaster, PA: DEStech Publications)
[14] Whitehouse D J 1976 Some theoretical aspects of error separation techniques in surface metrology *J. Phys. E: Sci. Instrum.* **9** 531–6
[15] Evans C J, Hocken R J and Estler W T 1996 Self-calibration: reversal, redundancy, error separation, and absolute testing *CIRP Ann.* **45** 617–34
[16] Grejda R D 2002 Use and calibration of ultra-precision axes of rotation with nanometer level *PhD Thesis* The Pennsylvania State University, USA
[17] Mitsui K 1982 Development of a new measuring method for spindle rotation accuracy by three points method *23rd Int. MTDR Conf.* pp 115–21
[18] Moore D 1989 Design considerations in multiprobe roundness measurement *J. Phys. E: Sci. Instrum.* **22** 339–43
[19] Zhang G X and Wang R K 1993 Four-point method of roundness and spindle error motion measurements *CIRP Ann.* **42** 593–6
[20] Zhang G X, Zhang Y H, Yang Z L and Li Z 1997 A multipoint method for spindle error motion measurement *CIRP Ann.* **46** 441–5
[21] Coorevits T and David J M 1991 Elimination of geometrical errors by permutations, application to a rotary table *CIRP Ann.* **40** 531–4
[22] Coorevits T 1990 Contribution au développement des techniques d'autocalibrage appliquées aux machines à mesurer tridimensionnelles *PhD Thesis* Arts et Métiers ParisTech, France
[23] Nouira H *et al* 2010 Investigation of the influence of the main error sources on the capacitive displacement measurements with cylindrical artifacts *J. Precis. Eng.* submitted
[24] Nouira H *et al* 2011 Evaluation of the capacitive displacement measurements in mechanical metrology with cylindrical artifacts *Proc. 13th Int. Conf. on Metrology and Properties of Engineering Surfaces* pp 300–4
[25] Smith P 2003 Analysis and application of capacitive displacement sensors to curved surfaces *MSME Thesis* College of Engineering at the University of Kentucky, USA
[26] Vissière A *et al* 2011 Experimental evaluation of the dissociated metrological technique (DMT) for the geometrical measurement in metrological applications *Proc. 13th Int. Conf. on Metrology and Properties of Engineering Surfaces* pp 394–8
[27] Vissière A *et al* 2010 Mesure géométrique avec une exactitude nanométrique *15th Int. Conf. of Metrology*
[28] David J M, Nouira H and Vailleau G P 2010 *Patent* (Laboratoire National de Métrologie et d'Essais LNE) on 'Dispositif et procédé de mesure de caractéristiques géométriques' no FR 1057394